In-orbit Demonstration of Reaction Control System for Orbital Altitude Change of Micro-Satellite ALE-2

Yuji Sato, Shinya Fujita, Yoshihiko Shibuya, Toshinori Kuwahara
Department of Aerospace Engineering, Tohoku University
6-6-11-304, Aramaki Aza Aoba, Aoba-ku, Sendai 980-8579, Japan; +81-22-795-5082
yuji.sato.b4@tohoku.ac.jp

Koh Kamachi
ALE Co., Ltd.
2-11-8 Shibadaimon, Minato-ku, Tokyo 105-0012, Japan; +81-3-6441-3312
koh.kamachi@star-ale.com

ABSTRACT

This research presents the results of an in-orbit test of the orbital altitude control for a micro-satellite equipped with the first space-demonstrated high-density small cold gas jet thruster. In the field of micro-satellites, the application of thrusters to practical missions has not yet progressed due to their high cost, mechanical and electrical incompatibility with the satellite bus system, and increased operational risks. By contrast, the demand for orbit control functions has been increasing in recent years with the expansion of micro-satellite applications. The 76 kg satellite "ALE-2", which was jointly developed by Tohoku University and ALE Co., Ltd., has the world's first challenging mission to artificially generate shooting stars by ejecting small substances (meteor source) from the ejection device fixed on the satellite body. To avoid collision of the ejected meteor source with other flying objects, the mission must be performed in a sun-synchronous orbit at an altitude of less than 400 km, which is lower than that of the International Space Station. However, it is required to maintain the mission orbit autonomously because the orbit decay is large due to the effect of atmospheric drag. In addition, to release the meteor source at an arbitrary orbital position, it is essential to manipulate the ground track by raising and lowering the orbital altitude. Therefore, ALE-2 needs to control the orbit altitude actively and with arbitrary amount of change. In this study, the reaction control system (RCS), which satisfies the orbit change capability, mission requirements, and compatibility with the satellite bus system, is installed on ALE-2 to perform space demonstrations of orbit control and to evaluate the operational performance of the thruster. ALE-2 will be the first to be equipped with a cold gas jet thruster developed by Patchedconics, LLC. It is estimated that the thruster is capable of changing altitude more than 1 km by continuous drive for one orbital period. Using this RCS, the following three criteria were set as the evaluation criteria: (Minimum) the orbit altitude can be actively changed by the thruster, (Full) the orbit altitude can be controlled by an arbitrary amount of operation and can be increased more than 1 km per orbit, and (Extra) the mission orbit can be transferred according to the meteor source release plan. ALE-2 was launched on December 6, 2019, and the in-orbit test of the RCS started four months later. Although the RCS was not able to achieve its initial orbit change capability due to an anomaly in the power supply system, various kinds of tests were conducted under conditions that allowed continuous thruster operation. It was confirmed that the orbit altitude was increased by 0.4 km per orbit. In addition, the fault detection, isolation and recovery (FDIR) function was effectively performed against any kinds of anomalies of RCS during in-orbit operation. Therefore, a sustained orbital altitude of 400 km was expected to be achievable using the onboard RCS.

INTRODUCTION

ALE project

ALE Co. Ltd. has the world's first challenging mission to artificially generate shooting stars by ejecting small substances (meteor source) from the ejection device fixed on the micro-satellite.[1,2] 400 small meteor particles of approximately 1 cm in diameter are loaded on a 50–100 kg scale satellite, and are launched backward one by one with high-pressure gas from an originally developed ejection device as shown in Figure 1. It is expected to be utilized for scientific applications such as compositional analysis of the middle atmosphere, detailed analysis of the meteor emission mechanism, and elucidation of the dynamics of re-entry objects. It also aims to create a space entertainment business. After the mission is accomplished, it is planning to hold a shooting star event at any time and place according to the customer's request.

Two satellites called “ALE-1” and “ALE2” have been jointly developed by ALE and the Space Robotics Laboratory (SRL) of Tohoku University, which is in

charge of the development of satellite bus system, as technical demonstrators for this mission. Figure 2 shows their appearance. They have been launched and are in operation. Table 1 describes their specifications.

Meteor source ejection may cause collision with other space vehicles, especially the International Space Station (ISS), or may become space debris. To avoid these risks, several measures are taken: (1) the orbit of the meteor source ejection is limited to 375–400 km, (2) risk assessment and planning based on the collision probability analysis with nearby flying objects should be conducted before the planning of the ejection, and (3) a double fail-safe system is used to detect deviations from the planned orbit and attitude and to safely suspend the meteor ejection during the release operation.[3] ALE-1 is equipped with a detachable membrane deployable orbit maneuvering system called Separable De-Orbit Mechanism (SDOM) for descent from an altitude of 500 km to below 400 km.[4] The descent started in December 2019. Although the SDOM can operate passively, the descent speed is unpredictable and affected by the space environment. The estimated time ranges from one to three years. Also, orbit raising is impossible. Since ALE-2 was released into a sun-synchronous orbit (SSO) at an altitude of approximately 400 km, mission operations could be performed without waiting for descent. However, active orbit control is required mainly for orbital maintenance.

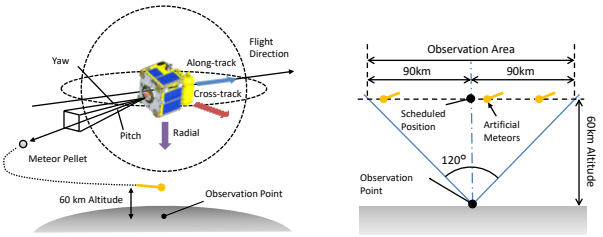

Figure 1: ALE Satellite Mission Overview

Figure 2: Flight Model of ALE-1 (left) and ALE-2 (right)

Table 1: ALE Satellite Specifications

	ALE-1	ALE-2
Size	W 570.0 × D 550.0 × H 720.0 mm	W 555.7 × D 656.2 × H 707.0 mm
Weight	68 kg	76 kg
Launch Date	January 18, 2019	December 6, 2019
Launcher	Epsilon-4th of JAXA	Electron of Rocket Lab
Initial Orbit	500 km SSO, LTDN = 9:30	400 km SSO, LTDN = 20:30
Orbit Control Method	Passive (A deployable and separable thin-film mechanism)	Active (A cold gas jet thruster system with 4 thrust nozzle)

Purpose of Orbit Control in ALE Satellite

For the safe execution of the artificial meteor ejection, the target orbit is set at an altitude of 375–400 km, which is lower than the ISS orbit. Since the atmospheric drag is dominant in this range of altitude, the orbit lifetime will be maintained by periodically conducting an orbit raising operation to extend the mission duration (at least one year compared to no action). In addition, to control the position and timing of the meteor ejection according to the customer's request, the orbit altitude is raised or lowered a few days to 30 days before the event to change the orbital period, and as a result, orbit transfer is performed to adjust the satellite passing area.

The required specifications and performance are as follows: (1) the orbital lifetime can be extended for about one year or more by maintaining the orbital altitude, (2) the meteor source emission event can be performed within a period of 30 days by selecting a specific point by adjusting the orbital altitude, and (3) the reaction control system (RCS) can be additionally installed on the existing bus system that has been used for the ALE-1 satellite. A cold gas jet with a total impulse of 1400 Ns and a wet mass of 9.3 kg was adopted to satisfy these requirements.

Application of Propulsion System for Micro-satellites

In the past, nano-satellites were rarely equipped with the propulsion system due to their limited payload resources. There is a trade-off between mission versatility and orbit change capability. It is also necessary to consider system safety, reliability, propellant handling, launch site operations, and development schedule.

With the diversification and expansion of missions, the demand for the RCS has increased. Meanwhile, the RCS has been downsized, upgraded, and optimized, so that it is no longer rare for micro-, nano-satellites and even CubeSats in recent years. Thrusters using chemical or electric propulsion with novel propellant materials that

emphasize non-toxicity and high efficiency, and thrusters of a small scale that can be mounted on CubeSats have been developed and performed in orbit.[5,6,7] However, they are still in their infancy, and many of them still have room for improvement in terms of reliability and functionality, as well as a lack of on-orbit experience.

Reaction Control System (RCS) for ALE-2 Micro-satellite

For the ALE-2 satellite, a high-efficiency cold gas jet thruster module developed by a Japanese venture company was adopted. This RCS meets the aforementioned performance requirements and is compatible with existing bus systems. The non-toxic propellant is also advantageous in terms of management, transportation, and ease of handling on launch site operations. This satellite is the first opportunity to demonstrate it in space.

The RCS was developed with maximum consideration of operational safety and system loss risk, and with high mission usability and minimum impact on the development schedule. The software logic to control the thrusters is simple, fast, and reliable based on general control methods.[8,9,10,11,12,13] Four thruster nozzles are arranged in the same direction and driven simultaneously to cancel torque and generate thrust in one axis direction. The thrust force is changed by the pressure controller on the RCS side, and no thrust feedback is provided on the satellite bus side. Attitude and angular velocity feedback control is conducted to change the direction of thrust and to compensate for the disturbance torque caused by the misalignment of the four nozzles with respect to the center of gravity of the satellite body. Such a control scheme is accomplished by off-pulse control of the four thrusters to simultaneously generate thrust and control attitude. In addition, the system automatically detects abnormalities such as increased spin speed due to malfunction of the thruster or sensors, and automatically separates and recovers the thruster, thereby improving operational safety and system reliability.

Research Objectives

This study aims to develop a thruster control system that can be installed on ALE-2, and to achieve an orbit altitude change of more than 1 km per orbit — by continuous operation of one orbital period — in order for the system to operate properly and meet the mission requirements. Once these goals are achieved, it will be easy to achieve arbitrary altitude orbit changes, orbit pass manipulations, and long-term and periodic orbit maintenance control. This space demonstration also serves as the operation verification of the first onboard thruster module. By verifying the functionality and usefulness of the thruster in this satellite, it is expected that this RCS module will be implemented in future micro- and nano-satellite missions and its performance will be further improved.

In this paper, the design of hardware, software and control operation plan for the RCS onboard the ALE-2 satellite is discussed. The soundness, performance and reliability of the designed and developed system were evaluated by simulations, electrical tests and system integration tests.

As a matter of fact, the original mission was not carried out because of the failure of the meteor source ejection mechanism after the launch of the ALE-2. However, the operation team was able to verify the on-orbit operation of the RCS and utilize it for the demonstration of orbit control. The problems that occurred in orbit were solved by changing the operation sequence and by using the autonomous fault detection, isolation, and recovery (FDIR) function effectively. This paper describes the results of the in-orbit thruster operation and its achievement evaluation with lessons learned in system development.

METHOD

ALE-2 Bus-system

ALE-2 is designed based on the ALE-1 bus-system. Figure 3 shows the system configuration. The mass budget of the system is shown in Figure 4. The RCS module including the propellant accounts for 9.3 kg (12.3%) of the 76 kg, while components for attitude and orbit control system (AOCS) occupies 10.8 kg (14.3%).

The Attitude Control Unit (ACU) is an on-board computer (OBC) that performs attitude and orbit control processing. ACU also manages the power distribution that provides from the Power Control Unit (PCU) and the communication link with subordinate attitude sensors and actuators. There are various types of attitude sensors and actuators as listed on Table 2, and placed as shown in Figure 5.

The Thruster Control Unit (TCU) mediates the power and the communication signal between the ACU and the thruster modules. It is used as an auxiliary OBC of the existing ACU. The TCU supplies power from the PCU and inputs it to the thruster via the step-up/step-down DC/DC converter and the FET-switch circuit. The control commands are generated in the ACU and are sent to the thruster control board via the TCU. The status of the thruster is received by the ACU via the TCU. The reason for this configuration is that we followed the policy of not modifying the existing bus system as much as possible, and also because the ACU detects thruster

abnormalities and disconnects it from the system, which has the advantage of preventing them from spreading to other sub-systems.

Table 2: List of AOCS Components

Category	Components
Sensors	Star Tracker (STT) Geomagnetic Sensor (GAS) Fine/Coarse Sun Aspect Sensor (FSS, SAS) Fiber Optic Gyroscope (FOG) MEMS Gyroscope (MEMSG) GPS Receiver (GPSR)
Actuators	Thruster Module Reaction Wheel (RW) Magnetic Torquer (MTQ)

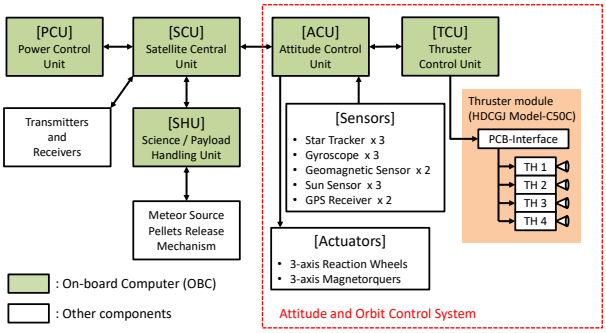

Figure 3: ALE-2 Bus-system Configuration

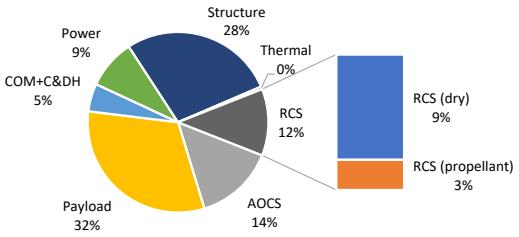

Figure 4: ALE-2 Mass Budget

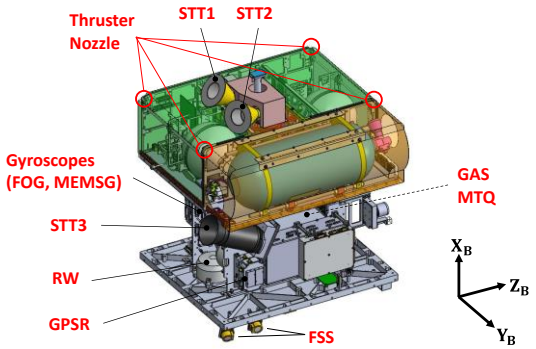

Figure 5: Arrangement of AOCS Components

Reaction Control System

ALE-2 is equipped with the High Density Cold Gas Jet System (HDCGJ) developed by Patchedconics, LLC.[14,15] Figure 6 shows an appearance of HDCGJ and Table 3 shows the summary of the specification. Figure 7 describes the arrangement of thruster nozzles. HDCGJ has 4 thruster nozzles that are attached in different directions and generate different reaction torques but the thrust force is the same (3 mN typical). Figure 8 shows the block diagram of this thruster module.

The direction vectors $\boldsymbol{r}_i$ [mm] and the thrust vector $\boldsymbol{f}_i$ [mN] (opposite to the injection direction) can be described as

$$r_1 = \begin{bmatrix} 281.36 \\ -236.47 \\ -274.77 \end{bmatrix},\ r_2 = \begin{bmatrix} 281.36 \\ -236.47 \\ 276.53 \end{bmatrix},\ r_3 = \begin{bmatrix} 281.36 \\ 102.33 \\ -274.77 \end{bmatrix},\ r_4 = \begin{bmatrix} 281.36 \\ 102.33 \\ 276.53 \end{bmatrix} \quad (1)$$

$$f_1 = f_2 = \begin{bmatrix} -3\cos 15^\circ \\ 0 \\ -3\sin 15^\circ \end{bmatrix},\ f_3 = f_4 = \begin{bmatrix} -3\cos 15^\circ \\ 0 \\ 3\sin 15^\circ \end{bmatrix} \quad (2)$$

The reaction torques $\boldsymbol{\tau}_i$ [μNm] can be described as

$$\boldsymbol{\tau}_i = \boldsymbol{r}_i \times \boldsymbol{f}_i \quad (3)$$

The thrusters are mounted on the $+X_B$ side of the satellite, and four thruster nozzles of the same shape are mounted. The opposing pairs are installed diagonally outward from each other, and THV-3 and 4 are positioned slightly closer to the center of gravity. This arrangement allows the thrust to be generated in the X_B direction and the control torque to be generated in the three axis directions.

The thrust is nominally 3 mN per unit, but the thrust can be increased to a maximum of 10 mN by controlling the tank pressure with heater control. To stabilize the thrust, a buffer tank is installed downstream of the main tank to store gas in a gas-liquid equilibrium state. Some heaters are driven to control the tank temperature and heat exchanger automatically. A valve upstream of the buffer tank is automatically opened and closed to keep the pressure within the target pressure range set on the RCS side, and the pressure in the buffer tank is maintained at a constant level.

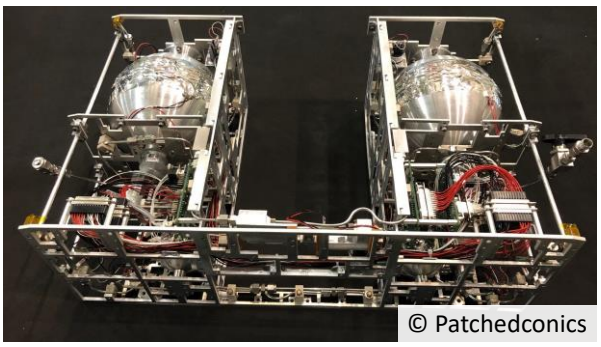

Figure 6: Thruster Module "HDCGJ Model-C50C"

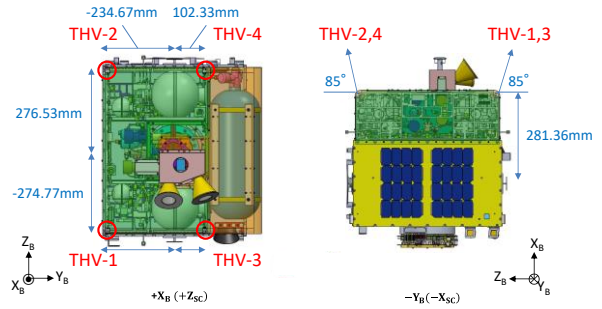

Figure 7: Thruster Nozzle Arrangement

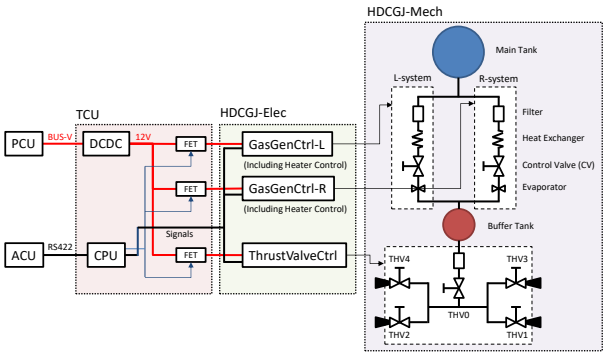

Figure 8: RCS Block Diagram

Table 3: RCS Specifications

Item	Value
Model Number	HDCGJ Model-C50C
Size	485 × 485 mm
Weight	7.3 kg (dry), 9.3 kg (wet)
Propellant	R600a (2 kg)
Number of nozzles	4
Thrust	3 mN (each nozzle, typ.)
Isp	70 s
Total Impulse	1400 Ns
Nozzle arrangement	See Figure 7 in detail
Operation Temperature	0–60 °C
Power consumption	10–24 W
Communication Type	UART (RS-422)

Orbit Control Strategy and Operation Plan

In order for ALE-2 to change its orbital altitude, it is necessary to drive the thrusters while keeping the thrust direction in the along-track (flight) direction as shown in Figure 9. For example, to increase the orbital altitude, the roll angle should be rotated 180° relative to the Local Vertical, Local Horizontal (LVLH) attitude. By driving the four thrusters, the resultant thrust is generated in the opposite of the flight direction, thus the altitude can be raised. On the other hand, when the orbit altitude is lowered, it should be fixed in the LVLH attitude. The reaction wheel cannot be used at the same time as the thruster because of the limitation of angular momentum storage and the strict power balance. The attitude maneuver is executed by appropriate on/off control of the four thrusters to guide to the desired attitude. Then, while maintaining the attitude by off-pulse control, the four thrusters are continuously driven to generate thrust in a constant direction. Considering the thruster configuration, THV-3 and THV-4 should be driven continuously, and THV-1 and THV-2 should be intermittently driven at a time ratio of 43% to maintain the attitude during active thrust generation. Assuming a single nozzle thrust of 3 mN, the maximum composite thrust (time-averaged) when using four nozzles is 8.32 mN. The thrust is output at a constant level by pressure control on the RCS side. The total ΔV is manually adjusted by the specified operation time.

In practice, the imbalance torque generated by each thruster (due to the discrepancy in its placement, the offset of the center of gravity, etc.) generates excess torque, which impedes continuous orbit control. In order to eliminate it, the reaction torque is generated by attitude feedback control to cancel the excess torque and modify the direction of thrust generation. Figure 10 illustrates the scheme described up to the present. The control algorithm that achieves the above is explained in the next section.

An operational plan is examined to change the altitude by continuous thruster control in one orbital period. Here, we consider orbit altitude ascent. If the same thrust is applied to raise the entire orbit evenly at all times, and impulse firing at perigee (altitude: h_1 [km]) and apogee (altitude: h_2 [km]) is replaced, the Hohmann orbit transfer equation can be applied and the following equation can be obtained:

$$\Delta V = \Delta V_p + \Delta V_a = \sqrt{\frac{\mu_{earth}}{r_1}}\left(\sqrt{2-\frac{r_1}{a}}-1\right)+\sqrt{\frac{\mu_{earth}}{r_2}}\left(1-\sqrt{2-\frac{r_2}{a}}\right) \quad (4)$$

where,

$$a = (r_1 + r_2)/2 \quad (5)$$

$$r_i = r_{\text{earth}} + h_{\text{i}} \quad (6)$$

$$\mu_{\text{earth}} = 3.986 \times 10^{15}\ [\text{km}^3/\text{s}^2] \quad (7)$$

$$r_{\text{earth}} = 6378.137\ [\text{km}] \quad (8)$$

The ΔV required to raise the altitude by 1 km can be calculated. According to Figure 11, ΔV = 0.566 m/s for an altitude of 400 km. On the other hand, the ΔV obtained by continuously driving the thruster for one revolution is calculated by the following momentum equation.

$$F\Delta t = m\Delta V \quad (9)$$

If F = 0.00832 [N], m = 75 [kg], Δt = 5553.6 [s], ΔV can be derived as 0.616 m/s. Therefore, orbit raising of more than 1 km is expected to be possible by continuous thruster drive for one orbital period. It is noted that the result will be a little worse if the excess torque cancellation due to torque imbalance is taken into account. Assuming that the orbit decay due to atmospheric drag at 390–400 km altitude is 3 km per month, the orbit life can be extended by about 11 months (= 33 orbital cycles) by periodically performing one orbit control every 10 days, considering the total propellant amount.

Next, let us consider changing the satellite passing area by changing the orbit altitude. At an altitude of 400 km SSO, the ground track moves about 2600 km per orbit. We calculated the change in the satellite pass position (measured at the equator) after N days with and without ΔV = 2.634 m/s (equivalent to propulsion control for 4 orbital cycles). It was found from Figure 12 that the change was 650 km after 16 days and 1300 km after 32 days. Therefore, the meteor source ejection event can be carried out within a period of about 30 days by selecting a specific point.

From the above discussion, it has been confirmed that the performance requirements of the ALE-2's mission can be satisfied without affecting both mission operation and bus system design and development, although some target values are not absolutely achieved.

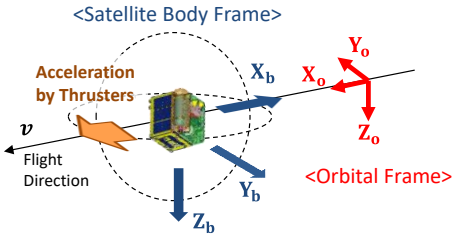

Figure 9: Coordinate System Definition

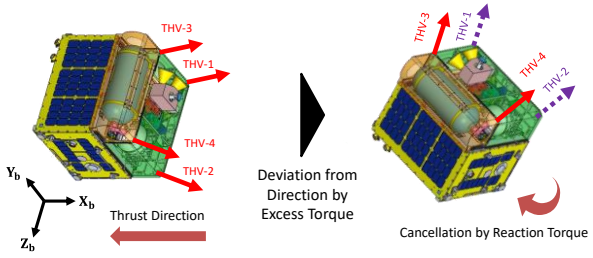

Figure 10: Thruster Operation Scheme

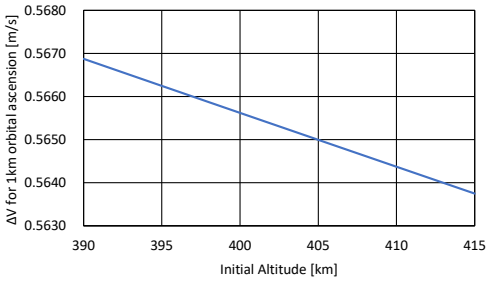

Figure 11: Delta V Required for 1-km Orbital Ascension

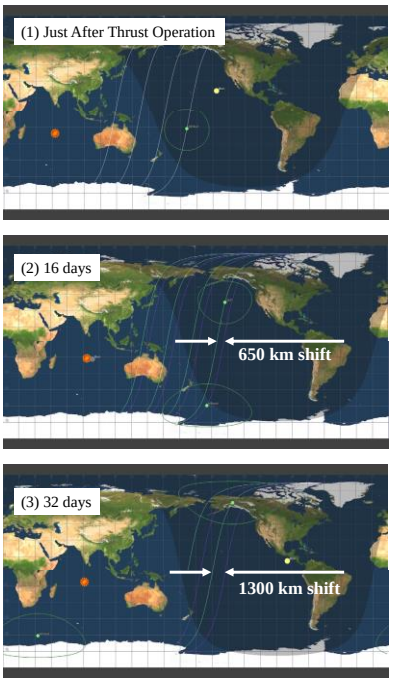

Figure 12: Satellite Pass Shift by Thrust Operation

Control Software

This section introduces the thruster control algorithm for simultaneous orbit and attitude control.[12,13,16] The logic is implemented on the ACU. The control block diagram is shown in Figure 13. The sensor measurement is performed at 20 Hz, while the calculation on the controller and the thruster command output are performed at 10 Hz.

The thruster is controlled by the following procedure. (I) From the attitude measurement results and the target attitude value, the targeted torque $\boldsymbol{T}_t$ is calculated based on the PID control law. (II) The targeted torque $\boldsymbol{T}_t$ is used to distribute thrust to each thruster and generate on/off pulses. The latter is further divided into the following processes: (II-A) Input the required torque $\boldsymbol{T}_t$ into a Schmitt trigger function that has a hysteresis characteristic and a dead zone for the purpose of

mitigating control instability, and determine the sign (+, 0, −). (II-B) Determine the nozzle opening/closing (on/off) combination of the four nozzles based on the sign of $\boldsymbol{T}_t$ by comparing it with the thruster nozzle switching table prepared in advance. (II-C) Control the nozzle open/close valves with a 10 Hz cycle using a pulse modulator such as Pulse-width Pulse-frequency modulator (PWPFM) to generate the required thrust for the time average and to optimize the valve open/close interval.

First, the required torque $\boldsymbol{T}_t$ is calculated by the following PID equation.

$$\boldsymbol{T}_t = K_p \boldsymbol{q}_e + K_d \boldsymbol{\omega}_e + K_i \int \boldsymbol{q}_e \, dt + \boldsymbol{\omega}_{sat} \times \boldsymbol{J}_{sat} \, \boldsymbol{\omega}_{sat} \quad (10)$$

Where, $\boldsymbol{q}_e (= \boldsymbol{q}_{\text{sat}}^{-1} \otimes \boldsymbol{q}_{\text{target}})$ is the attitude error, $\boldsymbol{\omega}_b (= \boldsymbol{\omega}_{\text{target}} - \boldsymbol{\omega}_{\text{sat}})$ is the angular rate error, K_p, K_d, and K_i are feedback gains, and $\boldsymbol{J}_{sat}$ is a satellite inertia tensor matrix. The first three terms on the right-hand side are the feedback terms of PID control, the fourth term is the feed-forward compensation term, and the fifth term is the cancellation term of gyro coupling. The attitude determination is estimated by the extended Kalman filter (EKF) using the magnetometer and gyroscope sensors. The target attitude value is calculated from the following equation.

$$\boldsymbol{q}_{\text{target}} = \text{DCMtoQuaternion}\left(\boldsymbol{C}_{\text{target}}\right) \quad (11\text{-a})$$

$$\boldsymbol{C}_{\text{target}} = \boldsymbol{C}_x(\phi)\boldsymbol{C}_y(\theta)\boldsymbol{C}_z(\psi)\boldsymbol{C}_{\text{orbit}} \quad (11\text{-b})$$

$$\boldsymbol{C}_{\text{orbit}} = [\boldsymbol{c}_0 \; \boldsymbol{c}_1 \; \boldsymbol{c}_2] \quad (11\text{-c})$$

$$\boldsymbol{\omega}_t = \{2\cos^{-1}(ds)/dT\} \, d\boldsymbol{v}/|d\boldsymbol{v}| \quad (12\text{-a})$$

$$d\boldsymbol{q} = [d\boldsymbol{v}, ds] = \boldsymbol{q}_{t(T-dT)}^{-1} \otimes \boldsymbol{q}_{t(T)} \quad (12\text{-b})$$

Where,
$\boldsymbol{c}_2 = -\boldsymbol{r}/|\boldsymbol{r}|, \boldsymbol{c}_1 = -\boldsymbol{r} \times \boldsymbol{v}/|\boldsymbol{r} \times \boldsymbol{v}|, \boldsymbol{c}_0 = \boldsymbol{c}_1 \times \boldsymbol{c}_2$,
$\boldsymbol{r}$: satellite position vector in ECI coordinate frame [m],
$\boldsymbol{v}$: satellite velocity vector in ECI coordinate frame [m/s],
φ : roll angle, θ : pitch angle, ψ : yaw angle [rad],
C_x, C_y, C_z: 3 × 3 rotation matrix.

Next, the process of generating on-off switching pulses for the thrusters is described. The method used in this satellite is very simple and does not require any on-board arithmetic. It controls four thrusters based on a preset nozzle allocation table. The nozzle allocation table is a table that maps the ON-OFF pattern of the four nozzles to the sign of the required torque $\boldsymbol{T}_t$. The table is designed to generate a torque close to the required generated torque $\boldsymbol{T}_t$ regardless of which nozzle on/off pattern is selected. In addition, different tables are chosen depending on the control purpose. For attitude control, the number of nozzles to be turned open is minimized to minimize excess thrust generation. On the other hand, the table that maximize the number of nozzles to be turned on is applied when the objective is orbit transfer. Since the required torque is generated at the same time, both orbit transfer and cancellation of excess torque can be performed without changing the control law itself and the definition of the table.

Let us take the thruster nozzle allocation table of the ALE-2 satellite as an example. Let the thrust vector (4×1) be $\boldsymbol{F}_{th}$ [mN] and the torque generated by each thrust vector (3×1) be $\boldsymbol{T}_{th}$ [μNm]. These two can be related by the following equation.

$$\boldsymbol{T}_{th} = \boldsymbol{B} \, \boldsymbol{F}_{th} \quad (13)$$

Where, $\boldsymbol{B}$ is called the thruster nozzle distribution matrix, and is calculated as follows.

$$\boldsymbol{B} = [\hat{\tau}_1 \; \hat{\tau}_2 \; \hat{\tau}_3 \; \hat{\tau}_4], \;\; \hat{\boldsymbol{\tau}}_{\text{i}} = \boldsymbol{r}_{\text{i}} \times \hat{\boldsymbol{f}}_{\text{i}} \quad (14)$$

The hat symbol means a variable with normalized thrust. In ALE-2,

$$\boldsymbol{B} = \begin{bmatrix} -60.737 & 60.737 & 26.485 & -26.485 \\ 192.586 & -194.286 & 192.586 & -194.286 \\ -226.674 & -226.674 & 98.843 & 98.843 \end{bmatrix} \quad (15)$$

Based on these equations, the combination of thruster nozzles and the total thruster torque can be expressed in Table 4. By referring this data, two types of nozzle allocation tables are created as shown in Table 5 and Table 6. The table type-A is built for attitude control (to minimize the total thrust), and the table type-B is built for orbit transfer control (to maximize the total thrust).

The advantage of using this control law is that it can be processed at high speed and is easy to implement in OBC. Since the control law provides attitude feedback, it is not affected by asymmetry or uncertainty in the thruster nozzle configuration, and is expected to be highly robust. On the other hand, since it is an on-off control, it is a non-optimal control and high propulsive efficiency is not expected. In addition, it requires a lot of time and effort to create tables in advance and to verify the effectiveness of the control.

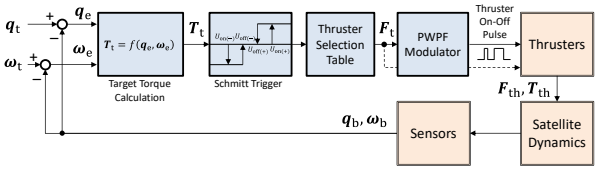

Figure 13: Thruster Valve Control Logic

Table 4: Combination of Thruster Nozzle and Total Torque

N *	F_{th} ** (THV-1,2,3,4)	T_{th} [μNm]		
		Roll	Pitch	Yaw
0	(0, 0, 0, 0)	0.00	0.00	0.00
1	(1, 0, 0, 0)	−60.74	192.59	−226.67
1	(0, 1, 0, 0)	60.74	−194.29	−226.67
1	(0, 0, 1, 0)	0.00	−1.70	−453.35
1	(0, 0, 0, 1)	26.48	192.59	98.84
2	(1, 1, 0, 0)	−34.25	385.17	−127.83
2	(1, 0, 1, 0)	87.22	−1.70	−127.83
2	(1, 0, 0, 1)	26.48	190.89	−354.50
2	(0, 1, 1, 0)	−26.48	−194.29	98.84
2	(0, 1, 0, 1)	−87.22	−1.70	−127.83
2	(0, 0, 1, 1)	34.25	−388.57	−127.83
3	(1, 1, 1, 0)	−26.48	−195.99	−354.50
3	(1, 1, 0, 1)	0.00	−1.70	197.69
3	(1, 0, 1, 1)	−60.74	190.89	−28.99
3	(0, 1, 1, 1)	60.74	−195.99	−28.99
4	(1, 1, 1, 1)	0.00	−3.40	−255.66

* N means the number of on-state thrusters.

** 0: off, 1: on. (1 mN in each thruster.)

Table 5: Thruster Nozzle Allocation Table Type-A (Smallest Thrust Configuration)

T_t,roll (+)		T_t,pitch		
		+	0	−
T_t,yaw	+	(0, 0, 1, 0)	(0, 0, 1, 1)	(0, 0, 0, 1)
	0	(0, 0, 1, 0)	(0, 1, 1, 0)	(0, 1, 0, 0)
	−	(0, 1, 1, 0)	(0, 1, 1, 0)	(0, 1, 0, 0)

T_t,roll (0)		T_t,pitch		
		+	0	−
T_t,yaw	+	(0, 0, 1, 0)	(0, 0, 1, 1)	(0, 0, 0, 1)
	0	(0, 0, 1, 0)	(0, 0, 0, 0)	(0, 0, 0, 1)
	−	(0, 1, 0, 1)	(1, 1, 0, 0)	(0, 1, 0, 0)

T_t,roll (−)		T_t,pitch		
		+	0	−
T_t,yaw	+	(0, 0, 1, 0)	(0, 0, 0, 1)	(0, 0, 0, 1)
	0	(1, 0, 0, 0)	(1, 0, 0, 1)	(0, 0, 0, 1)
	−	(1, 0, 0, 0)	(1, 0, 0, 0)	(0, 1, 0, 0)

Table 6: Thruster Nozzle Allocation Table Type-B (Largest Thrust Configuration)

T_t,roll (+)		T_t,pitch		
		+	0	−
T_t,yaw	+	(0, 0, 1, 0)	(0, 0, 1, 1)	(0, 0, 0, 1)
	0	(1, 1, 1, 0)	(0, 1, 1, 0)	(0, 1, 1, 1)
	−	(1, 1, 1, 0)	(0, 1, 1, 0)	(0, 1, 1, 1)

T_t,roll (0)		T_t,pitch		
		+	0	−
T_t,yaw	+	(0, 0, 1, 1)	(0, 0, 1, 1)	(0, 0, 0, 1)
	0	(0, 0, 1, 1)	(0, 0, 1, 1)	(0, 0, 0, 1)
	−	(1, 0, 0, 0)	(1, 1, 0, 0)	(1, 1, 1, 1)

T_t,roll (−)		T_t,pitch		
		+	0	−
T_t,yaw	+	(0, 0, 1, 0)	(0, 0, 1, 1)	(0, 0, 0, 1)
	0	(1, 0, 1, 1)	(1, 0, 0, 1)	(1, 1, 0, 1)
	−	(1, 0, 1, 1)	(1, 0, 0, 1)	(1, 1, 0, 1)

Fault Detection, Isolation and Recovery (FDIR) function

We have implemented a mechanism in the OBC software that can detect, isolate, and recover from anomalies of the RCS by identifying possible operational hazards in advance. The flowchart is shown in Figure 14. For example, we identified the following hazards: housekeeping (HK) transmission stoppage due to an abnormality in the electrical system of RCS module, a sudden increase in spin speed due to an abnormality in the valve system, an abnormality in the output of the attitude sensor, and an abnormality in the attitude control calculation (due to a parameter setting error). The output anomaly of the attitude sensor is considered to be an anomaly when the angular velocity sensor measurement value exceeds the threshold (= 0.6°/s in the norm value) or the output is stopped, and the angular error between the geomagnetic field vector analogized from the attitude determination value and the measured geomagnetic field vector exceeds the threshold (= 10°). If these anomalies continue for a certain period of time (0.1–6553.5 s), a thruster stop command is automatically sent out, and then the main power of the thruster is cut off to return the satellite system to a safe state.

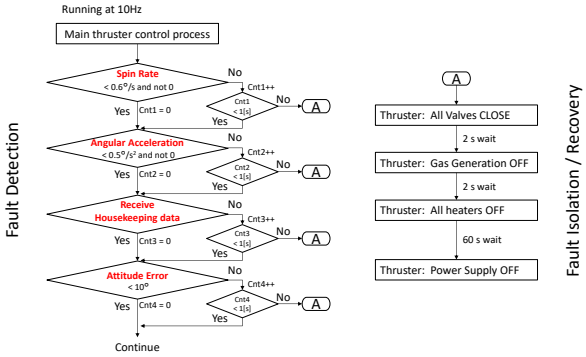

Figure 14: FDIR Flowchart for RCS Anomaly

Closed-loop Control Simulation

In order to evaluate the effectiveness of the control algorithm proposed in the previous section, software simulations were conducted based on the environment of the software-in-the-loop (SIL) system. This research uses the Satellite and Space Environment Simulator (SSES), which is a dynamics simulator owned by the SRL.[17] Sensors, actuators, and OBCs are represented as mathematical models, which are connected to the dynamics computer to construct a closed-loop control system. The model is constructed based on the operational data of the equipment and the ground measurement data, which have been proven in ALE-1, and can reproduce, for example, vibration transmission delay, sensor noise, mounting angle offset, power consumption, etc. The contents of the OBC model are identical at the function level to the program written to the actual CPU. The attitude dynamics equation is as follows.

$$\dot{\boldsymbol{H}} + \boldsymbol{\omega}_{sat} \times \boldsymbol{H} = \boldsymbol{T}_{th} + \boldsymbol{T}_{mtq} + \boldsymbol{T}_{disturb} \tag{16}$$

$$\boldsymbol{H} = \boldsymbol{J}_{sat}\boldsymbol{\omega}_{sat} + \boldsymbol{h}_{rw} \tag{17}$$

$$\dot{\boldsymbol{q}} = \frac{1}{2}\boldsymbol{\Omega}_{\mathrm{sat}}\boldsymbol{q},\ \boldsymbol{\Omega} = \begin{bmatrix} 0 & \omega_z & -\omega_y & \omega_x \\ -\omega_z & 0 & \omega_x & \omega_y \\ \omega_y & -\omega_x & 0 & \omega_z \\ -\omega_x & -\omega_y & -\omega_z & 0 \end{bmatrix} \tag{18}$$

where $\boldsymbol{T}_{mtq}$ is generated torque by the magnetic torquer, $\boldsymbol{T}_{disturb}$ is disturbance torque, and $\boldsymbol{h}_{rw}$ is angular momentum of reaction wheels.

The experimental conditions are defined as the design parameters close to the actual ALE-2 satellite, and the control gain is adjusted. Table 7 shows the simulation parameters. The simulation results (from Figure 15 to Figure 19) showed that the attitude error was within ±3°, the orbit altitude change was +1.058 km, total ΔV was +0.574 m/s, and the propulsion control efficiency was 93.2%. In the case of applying a center-of-gravity offset, control to compensate for the disturbance torque caused by the offset is also necessary. Therefore, the attitude error was within ±4°, the orbit altitude change is +0.827 km, and the propulsion control efficiency was reduced to 71.4% if the center-of-gravity offset is given as {+30, +30, +30} mm. Nevertheless, the control is executed normally and the robustness against mechanical disturbances is confirmed by this result.

Table 7: Simulation Condition

Item	Parameters
Initial orbital elements	$\boldsymbol{r}_{eci}$ = { 4216.49, −5183.92, 1194.77 } [km] $\boldsymbol{v}_{eci}$ = { −1.572, 0.449, 7.487 } [km/s]
Initial attitude	$\boldsymbol{q}$ = { 0, 0, 0, 1 }
Initial angular rate	$\boldsymbol{\omega}$ = { 0.2, 0.2, 0.2 } [°/s]
Simulation time	From 22:52:00 UTC, Mar. 23, 2020 3 hours for thruster control operation
Thruster control cycle	10 Hz interval
Thruster control gain (X,Y,Z)	K_p = { 5000, 5000, 5000 } K_d = { 300000, 300000, 300000 } K_i = { 0, 0, 0 } K_f = { 2160, 2110, 2120 }
Thruster control dead band threshold (X,Y,Z)	U_{on} (+) = { 200, 200, 200 } U_{off} (+) = { 50, 50, 50 } U_{on} (−) = { −200, −200, −200 } U_{off} (−) = { −50, −50, −50 }
Thruster control delay	50 ms

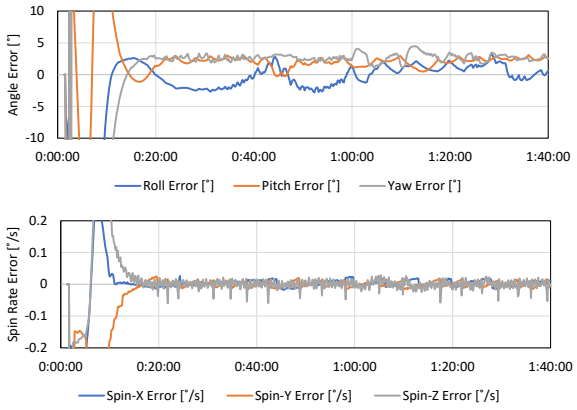

Figure 15: Simulation Result (Attitude Error, Angular Rate Error)

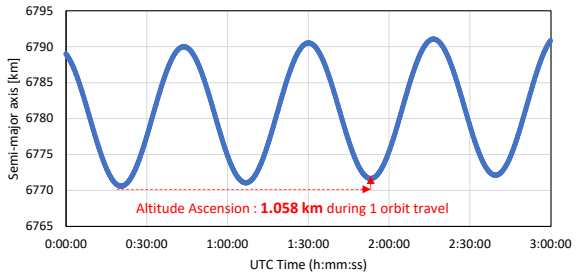

Figure 16: Simulation Result (Altitude Change)

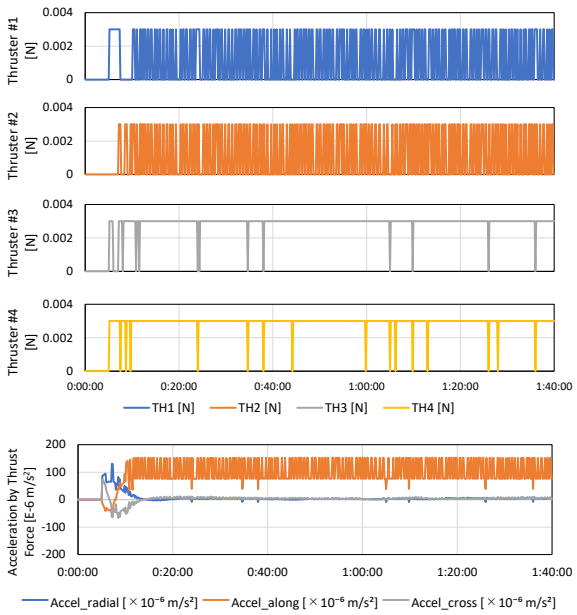

Figure 17: Simulation Result (Thrust, Acceleration)

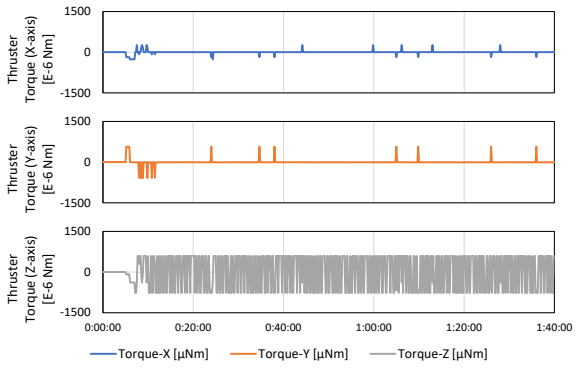

Figure 18: Simulation Result (Total Torque)

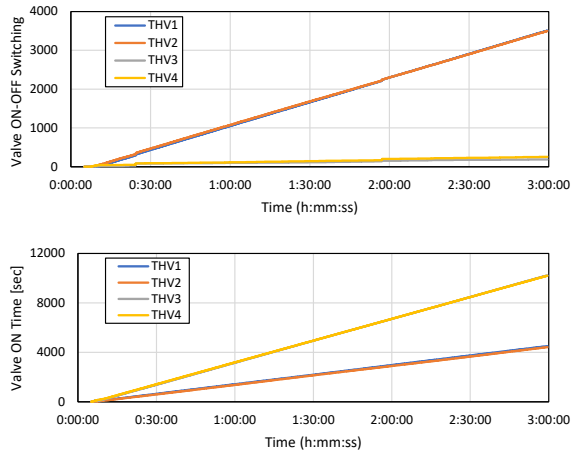

Figure 19: Simulation Result (Valve Control)

On-ground integration test

To confirm the functionality of RCS hardware and control software, various kinds of test were conducted: Hardware-in-the-loop (HIL) test for verification of OBC, electrical test for RCS module itself, and system integration test including the compatibility check with power supply system, communication, and mechanical environment.

In the HIL test, the virtual sensor data generated by the simulator is input to the actual OBC, and the thruster drive signal is returned back to the simulator to perform dynamics calculation. The purpose is to evaluate the implemented program of the OBC and to check the operation of the communication process with peripheral devices. Figure 20 describes the configuration of HIL simulation.[16,17] The OBC model used in the SIL simulator described above was replaced with the actual device, and a dedicated input/output interface for the OBC was constructed using the PCI eXtensions for Instrumentation (PXI) system provided by National Instruments. As for the results of the evaluation, the OBC system can be judged to be normal because the same results were obtained compared to the SIL simulation result. In addition, when the simulator intentionally created an abnormal situation (e.g., disconnection of equipment, sudden increase in spin, etc.), the OBC was able to detect it and shut down the RCS in the expected sequence.

In the electrical test, we evaluated whether the heaters (attached on 3 tanks and a heat exchanger) and solenoid valves could be commanded from the OBC and whether the status of temperature and pressure could be obtained normally. Figure 21 shows the test in progress. As a result, an abnormal phenomenon was found in which some of the solenoid valves did not open properly when four or more of them were tried to open simultaneously. The reason for this is that a spike current of several A/valve is generated when the solenoid valve is driven, which prevented the proper supply of power. The problem was avoided by turning open two of the four valves first and then turning open the other two valves after 0.05 s interval.

In the system integration test, the communication, power supply, and structural compatibility were evaluated in the final state with the RCS mounted on the main body of the satellite. There were no abnormalities in the communication and power supply. However, we did not conduct a long-term operation test. Although the thruster was powered by a solar cell simulator (simulating sunshine) and a satellite battery (simulating eclipse) to simulate the real situations, the number of trials and the degree of electrical load were both small. The lack of

testing here would later become as a problem during operation.

In terms of the structure, several problems were found after the vibration test, such as the disconnection of the piping fixture. Therefore, additional reinforcement was applied. No change or abnormality was found in the electrical and thrust characteristics after the vibration test.

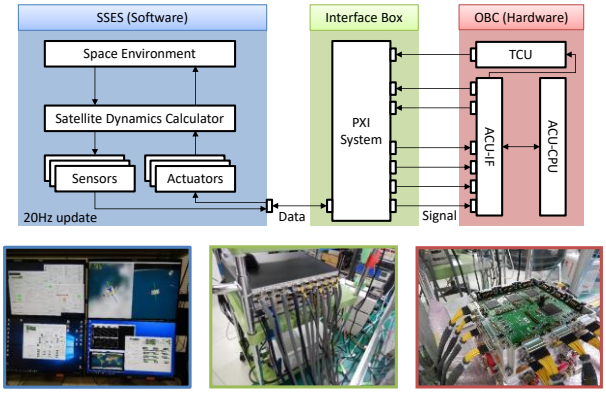

Figure 20: Configuration of HIL Simulation

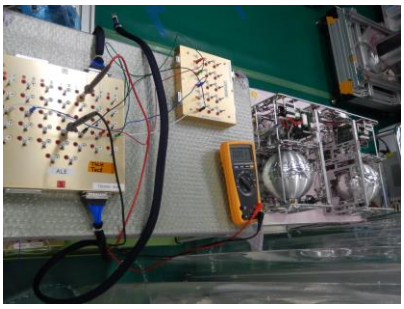

Figure 21: Electrical Test of RCS Module

RESULT AND DISCUSSION

Measurement of Thruster Operational Performance

As an initial phase of operation, the thruster thrust characteristics was evaluated. The output thrust can be changed by changing the target pressure setting. The thrust force was estimated from the rotational behavior of the satellite when the thruster was operated in a certain time. The relationship between the set pressure and output thrust was obtained as shown in Figure 22.

The nozzle position vector and thrust vector will deviate from the design values due to factors such as misalignment of the four thruster nozzles and deviation of the arm length due to the offset of the center of gravity of the satellite body. To evaluate the degree of deviation, the torque matrix was estimated from the change in the angular momentum accumulation of the reaction wheel. The result shows that the torque imbalance between THV-3/4 is very large, and the gap is relatively 24–35% stronger for THV-4 (illustrated in Figure 23, based on the measured data on March 24, 2020). The torque imbalance is compensated by the control as mentioned before, that means this problem is not serious. The problem is that the burden is concentrated on a specific valve, and because extra torque is created to compensate, the control capability cannot be demonstrated 100%, resulting in a decrease in control efficiency.

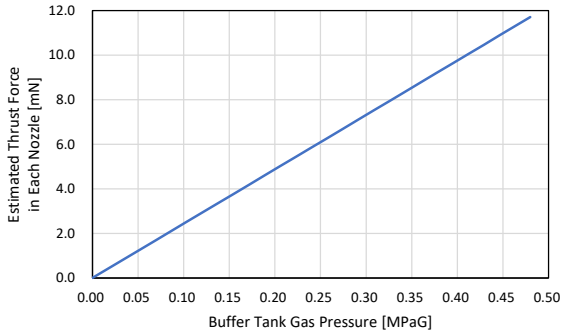

Figure 22: RCS Performance (Pressure vs. Thrust)

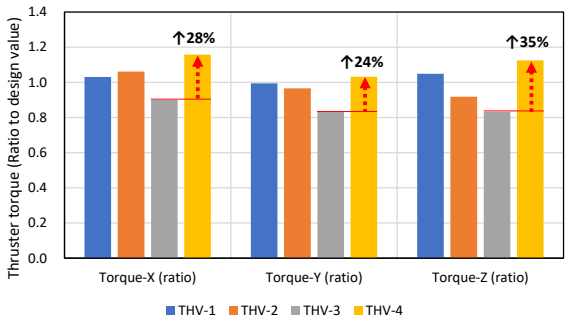

Figure 23: Imbalance of Thruster Torque

In-orbit Demonstration of Orbit Control

Table 8 and Figure 24 show the definition of the operation sequence and the test condition. For the reasons described below, we decided to control the RCS for a half orbital cycle (35–45 minutes). In order to make the thrust direction along the flight direction first, only attitude control using the thrust minimization table was performed during the 10-minute period, followed by 35-minute orbital transfer operation.

The test results described in Figure 25 and Figure 26 showed that the attitude angle was within ±4° and the rotation rate was within ±0.06°/s. It was confirmed in another test that the steady deviation of the attitude angle could be improved by introducing the I-control. In addition, it was confirmed through several experiments that control was possible regardless of the initial value of the attitude and regardless of the thrust level.

Along with the above results, the thruster HK data that includes the temperature and tank pressure, the thruster operation time and the number of open/close switches are shown in Figure 27, Figure 28 and Figure 29 respectively. The buffer tank pressure is maintained at a predetermined level, and the temperature keeps decreasing from the middle because of the long drive time, and the heater operates at 5℃, which is close to the vapor pressure temperature, and the temperature is controlled to be maintained at the same level.

Next, a total of five trials were conducted over a one-month period from October to November 2020, changing some of the operational conditions that is described in Table 9. We also changed the thrust level and control time, and evaluated the degree of orbit raising due to the increase in thrust. As a result, we succeeded in raising the orbit by +1.342 km, compared to the expected decay of −0.532 km in one month as shown in Figure 30. The real propulsive efficiency (the ratio of the theoretically expected ΔV under the relevant operational conditions and parameters to the actual ΔV based on the recorded drive data) was around 80%. The efficiency dropped to around 50% at high thrust case. The causes of this are enlargement of influence by torque imbalance (between THV-3 and 4), deviation of the attitude angle, and instability of the generated thrust, however, details are still under analysis.

Table 8: In-orbit Test Condition (Single)

Item	Parameters
Operation time	21:32:00 UTC, Nov. 16, 2020
Operation sequence	21:32:00 UTC: (−0:08:00) Start preliminary attitude control 21:40:00 UTC: (+0:00:00) Switch to orbital ascending control 22:15:00 UTC: (+0:35:00) Stop thruster control All sequence is conducted at sunshine.
Thruster gas control	Enabled, within 0.223–0240 MPaG
Thrust level	Approximately 5.85 mN in each nozzle
Thruster control cycle	10 Hz interval
Thruster control gain (X,Y,Z)	K_p = { 5000, 5000, 5000 } K_d = { 300000, 300000, 300000 } K_i = { 0, 0, 0 } K_f = { 2160, 2110, 2120 }
Thruster control dead band threshold (X,Y,Z)	U_{on} (+) = { 200, 200, 200 } U_{off} (+) = { 50, 50, 50 } U_{on} (−) = { −200, −200, −200 } U_{off} (−) = { −50, −50, −50 }

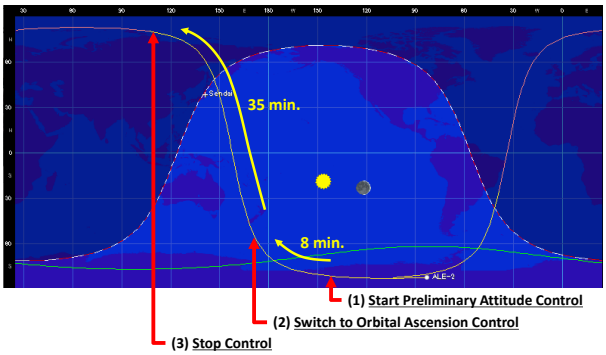

Figure 24: Thruster Operation Sequence

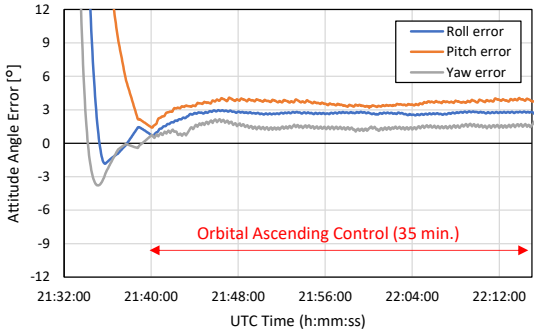

Figure 25: Test Result (Attitude Error)

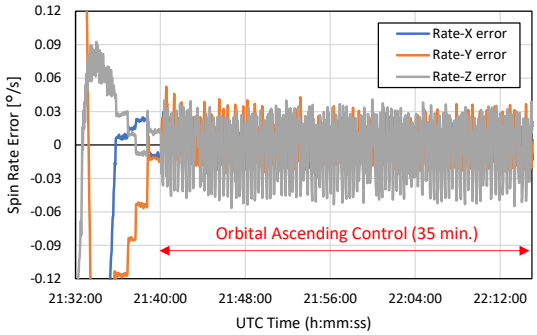

Figure 26: Test Result (Angular Rate Error)

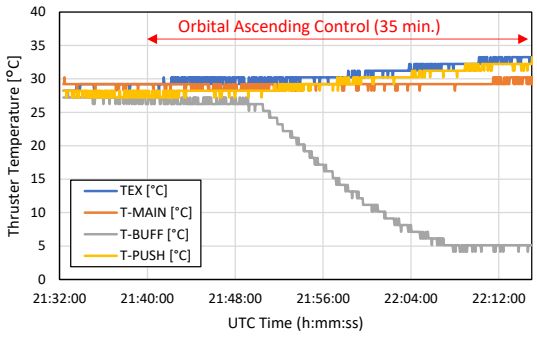

Figure 27: Test Result (Temperature)

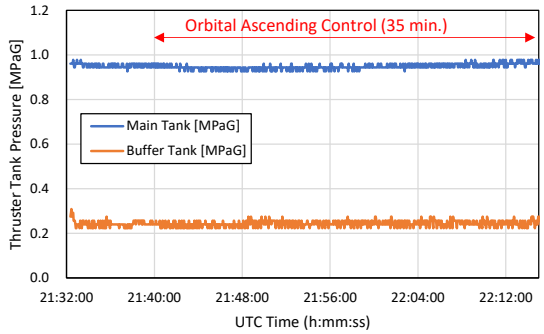

Figure 28: Test Result (Tank Pressure)

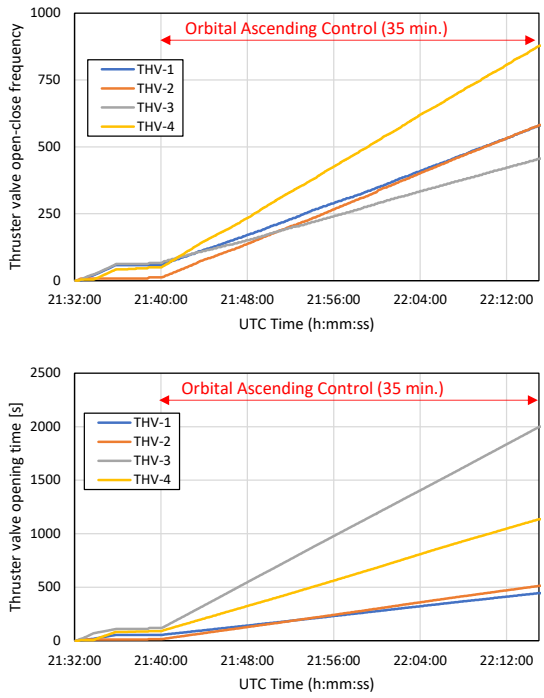

Figure 29: Test Result (Valve Control)

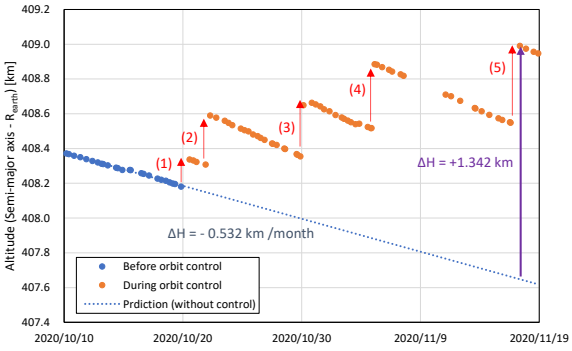

Figure 30: In-orbit Test Result (Altitude Change)

Table 9: In-orbit Test Result (5 Trials in a Month)

#	Date	Thrust	Control Time	Altitude Change	Effici-ency
(1)	Oct. 19	2.1 mN	22.5 min.	+156 m	85.5%
(2)	Oct. 21	2.1 mN	45 min.	+282 m	76.9%
(3)	Oct. 29	2.1 mN	45 min.	+294 m	80.3%
(4)	Nov. 4	3.75 mN	45 min.	+368 m	56.2%
(5)	Nov. 16	5.85 mN	35 min.	+442 m	55.7%

Lessons Learned – Anomaly Handling and Operational Constraints

This section describes a lessons learned about the anomaly handling and operational constraints.

The anomalies that occurred: The logic-circuit power of the RCS fails immediately after the valve is driven in a shaded area, making it impossible to continue control. Specifically, when the battery (BAT) is discharged and the voltage drops below 12 V, the logic power supply fails during valve drive with high probability. In addition, if the valve drive frequency is high (3–4 valves are open on average), the logic-circuit power supply will fail within a few minutes regardless of the BAT voltage.

Cause: The step-up/step-down DC/DC 12 V power supply of the TCU seems to be unstable when the load is high or the supply voltage is low. When the output voltage drops below a certain level, the CPU of the logic circuit is reset and the power is not turned on again. Since all valves are closed when the power is cut off, there is no safety problem. When the RCS is restarted manually, the system returns to normal operation. To recognize this problem in advance, repetitive tests and long-term operation tests should have been certainly performed in the electrical tests on the ground.

Countermeasures and constraints: (1) Drive the thruster in daylight and with the BAT voltage charged to 12 V. (2) The valve drive frequency should be reduced (less than three valves opening on average). For (1), the thruster control time is limited to 65 minutes after the start of the daylight region. For (2), the thruster table will be rearranged so that only attitude control will be performed for the first 10 minutes to stabilize the attitude and direct the thrust with minimum thrust, and pulse control will be performed for the next 45 minutes to generate active thrust. Note that if the orbital altitude is to be raised, this operation must be performed in the vicinity of the apogee and the perigee must be raised. In the worst case, the propulsive efficiency will be reduced by 1/4 of the theoretical value because the time average will be reduced from 3–4 to 2 and the orbit will be controlled halfway around the Earth.

Effects: The results show that the hardware problem that is mentioned above was solved by changing the operation plan and reconfiguring the thruster table, although the operational constraints became more severe.

Lessons Learned – Application of FDIR function

This section reports the operation result of the pre-implemented FDIR function in response to the abnormal events of the RCS.

The anomalies that occurred: The FDIR function can deal with these anomalies: HK transmission stop of the thruster (caused by the BAT supply voltage drop mentioned above), accidental output anomaly of the attitude sensor, and attitude control calculation anomaly (caused by parameter setting error), which are the hazards that were assumed in advance. For example, it was reported that the sun sensors could not measure the sun vector properly when the control started too early after the satellite entered the sunshine area, so the control started with the wrong attitude measurement value and normal thrust direction control could not be performed. As a countermeasure, it is possible to measure the sun vector normally if the control is delayed to 5 minutes after the start of daylight. Nevertheless, an anomaly may occur depending on the initial attitude.

Countermeasures and effects: The FDIR function worked effectively for all anomalies, and the RCS itself was protected from anomalies without spreading to other systems, avoiding higher risks such as power depletion, attitude recovery difficulties due to increased spin, and deviation from the mission orbit.

To be improved: After an abnormal stop, the RCS is powered down only and not restarted automatically. Considering the operation management, it was an option to restart the system automatically. In addition, the system does not cover all the hazards such as anomalies in pressure control. It needs to be further improved by reflecting the operation results of ALE-2.

CONCLUSION

Although the artificial shooting star ejection micro-satellite ALE-2 has not achieved its main mission due to the malfunction of the ejection equipment, the orbit control technology was successfully demonstrated using the high-efficiency cold gas jet thruster developed by a Japanese venture company, which is the first space demonstration product. The satellite bus-system is designed to meet the following mission requirements for the ALE-2 satellite: (1) the orbital lifetime can be extended for about one year or more by maintaining the orbital altitude, (2) the meteor source emission event can be performed within a cycle of 30 days by selecting a specific point by adjusting the orbital altitude, and (3) the system can be added to the existing bus system that has been proven in the ALE-1 satellite. The proposed hardware, software, and operation strategy satisfied all of the mission requirements. On the other hand, the results of the on-orbit demonstration showed that the system was not able to achieve the ±1 km altitude transfer by continuous drive in one orbital period, which is necessary to satisfy these requirements. This was caused by inadequacies in the design and ground test of the power supply system of the satellite bus. By devising the operation sequence and changing the parameters appropriately, we succeeded in adding an orbit change of up to ± 0.4 km by continuously driving the thruster halfway around the orbit in the daylight region. In other words, if the number of orbit cycles using the thruster will increase, the required objectives of extending the orbit lifetime and adjusting the satellite ground pass are expected to be feasible. In addition, the FDIR function was effectively activated against any kinds of failures during in-orbit operation, and a high level of operational safety was secured. We will continue to perform the orbit maintenance control — hoping for the possibility of recovery of the ejection system — and utilize the operational data for further improvement of the thruster control performance.

Acknowledgments

The authors are grateful to ALE Co., Ltd. and Patchedconics, LLC for their technical support.

References

1. Kamachi, K., Shibuya, Y., Oikawa, Y., Yamada, S., Imura, S., Arisaka, I., et al., “Mission Planning for Artificial Shooting Star and Risk Assessment,” Proceeding of 62nd Space Science and Technology Conference, Kurume, Japan, October 24–26, 2018, JSASS-2018-4147 (in Japanese).
2. Shibuya, Y., Sato, Y., Tomio, H., Kuwahara, T., Fujita, S., Kamachi, K., et al., “Development and Demonstration of the Mission Control System for Artificial Meteor Generating Micro satellites,” 2021 IEEE/SICE International Symposium on System Integration (SII), Iwaki, Fukushima, Japan, January 12–15, 2021, WeD2.1.
3. Fujita, S., Sato, Y., Kuwahara, T., Sakamoto, Y., Shibuya, Y., and Kamachi, K., “Double Fail-Safe Attitude Control System for Artificial Meteor Microsatellite ALE-1,” Transactions of the Japan Society for Aeronautical and Space Sciences, Aerospace Technology Japan, Vol. 19, No. 1, pp.9–16, 2021.
4. Pala, A., Kuwahara, T., Honda, T., Uto, H., Kaneko, T., Potier, A., et al., “System Design, Development and Ground Verification of a

Separable De-Orbit Mechanism for the Orbital Manoeuvre of Micro-Satellite ALE-1," Transactions of the Japan Society for Aeronautical and Space Sciences, Aerospace Technology Japan, Vol. 19, No. 3, pp.360–367, 2021.

5. Dinardj, A., Anflo, K., and Friedhoff, P., "On-Orbit Commissioning of High Performance Green Propulsion (HPGP) in the SkySat Constellation," 31st Annual AIAA/USU Conference on Small Satellites, SSC17-X-04, 2017.
6. Koizumi, H., Komurasaki, K., and Arakawa, Y., "Development of the Miniature Ion Propulsion System for 50 kg Small Spacecraft," 48th AIAA/ASME/SAE/ASEE Joint Propulsion Conference & Exhibit, 2012.
7. Levchenko, I., Bazaka, K., Ding, Y., Raitses, Y., Mazouffre, S., Henning, T., et al., "Space micropropulsion systems for Cubesats and small satellites: From proximatetargets to furthermost frontiers," Applied Physics Reviews, 5, 011104, 2018.
8. Oland, E., "Modeling and Attitude Control of Satellites in Elliptical Orbits," In book: Applied Modern Control, IntechOpen, November 2018.
9. Mazinan, A. H., Pasand, M., and Soltani, B., "Full Quaternion Based Finite-time Cascade Attitude Control Approach via Pulse Modulation Synthesis for a Spacecraft," ISA Transactions, 58, pp.567–585, 2015.
10. Fazlyab, A., Ajorkar, A., and Kabganian, M., "Design of an Adaptive Controller of a Satellite using Thruster Actuator," International Journal of Computer Applications, Vol. 102, No. 10, pp.6–12, 2014.
11. Silva, N., Delpy, P., and Ducarouge, A., "Three DOF Optimal Thrusters Selection and Modulation for Space Vehicles," IFAC Proceedings Volumes, Vol. 37, Issue 6, pp.149–154, 2004.
12. Nada, Y., and Kawaguchi, J., "Attitude and orbit control law using four thrusters for ALEx satellite," 29th Workshop on JAXA, Astrodynamics and Flight Mechanics, ISAS/JAXA Sagamihara, Japan, July 22–23, 2019, C-15 (in Japanese).
13. Sato, Y., Fujita, S., Kuwahara, T., Shibuya, Y., Kamachi, K., Kawaguchi, J., et al., "Design and Evaluation of Thruster Control Approach for Micro-satellite ALE-2," 2020 IEEE/SICE International Symposium on System Integration (SII), Honolulu, Hawaii, USA, January 12–15, 2020, Mo3B.6.
14. Ohashi, K., Kawaguchi, J., and Kubo, Y., "Development of High Density Cold Gas Jet Propulsion System for Micro Satellites," 29th Workshop on JAXA, Astrodynamics and Flight Mechanics, ISAS/JAXA Sagamihara, Japan, July 22–23, 2019, C-16 (in Japanese).
15. Padovan, T., Kawaguchi, J., "Heater-Free, Lowest Power Consumption & Highest Volume Availability Gas-Generator Propulsion System - Most Suitable for Micro to Nano Satellites," 35th Annual AIAA/USU Conference on Small Satellites, 2021 (Accepted in the poster session).
16. Sato, Y., Fujita, S., Kuwahara, T., Shibuya, Y., and Kamachi, K., "Design, Implementation and In-orbit Demonstration of Attitude and Orbit Control System for Micro-satellite ALE-2," 2021 IEEE/SICE International Symposium on System Integration (SII), Iwaki, Fukushima, Japan, January 12–15, 2021, Mo3B.6.
17. Sato, Y., Fujita, S., Kuwahara, T., Honda, T., Sakamoto, Y., Shibuya, Y., et al., "Establishment of the Ground Evaluation and Operational Training System of Artificial Meteor Micro-satellite ALE-1," Transactions of the Japan Society for Aeronautical and Space Sciences, Aerospace Technology Japan, Vol. 18, No. 3, pp.84–92, 2020.